ICM11

Implementation of the GTN Damage Model to Simulate the Small Punch Test on Pre-Cracked Specimens

J. M. Alegre[a]*, I. I. Cuesta [a], P.M. Bravo[a]

aCivil Engineering Department, University of Burgos, E.P.S., C/ Villadiego s/n, 09001 Burgos, Spain

Abstract

Nowadays, pre-cracked Small Punch Tests (P-SPT) are used in those cases where there is not enough material for conducting conventional tests. In this paper, P-SPT has been used to determine the fracture properties of the 15.5PH steel, using the micromechanical model, developed by Gurson-Tvergaard-Needleman (GTN). The effect of variation of damage parameters on the numerical simulation has been analyzed. This numerical simulation is based on the sequential adjustment of the experimental load-displacement curves obtained from P-SPT. Interrupted test have been also developed in order to know the cracking process during loading and the damage evolution until fracture.

Selection and peer-review under responsibility of ICM11

Keywords: Small Punch Test; Pre-cracked Specimen; Gurson-Tvergaard Damage Model, Ductile Fracture, Interrupted Test, 15.5PH steel.

1. Introduction

In those cases where there is not enough material for conducting conventional tests to determine the mechanical properties of the material analyzed, there are now several non-standard tests that will achieve this purpose. One of them is the Small Punch Test (SPT) [1-3], which basically consists of deforming a miniature specimen using a high-strength punch, while the sides of the specimen are firmly held between two dies.

One of the greatest challenges at present is to obtain the fracture properties of a material from this type of test. Most of papers on this topic have until now used conventional SPT specimens and only few authors have utilized pre-cracked specimens (P-SPT) [4-6]. To achieve this initial crack in the P-SPT specimen prior to fracture testing, two procedures are mainly being used at present. The first one uses high-precision micromachining (HPM), and the second relies on laser-induced micromachining (LIM).

The main objective of this work is to apply the Gurson-Tvergaard damage model to simulate the load-displacement curve obtained from the P-SPT, and to establish a methodology for obtaining the constitutive parameters of the material from the stages observed in the P-SPT. This model simulates the material behaviour from the initial elastic behaviour until its failure considering the nucleation, growth and coalescence of microvoids.

---

* Corresponding author. Tel.: +0-34-947259420; fax: +0-34-947259485.
E-mail address: jalegre@ubu.es.

Nomenclature

a	Initial crack size, *mm*
D_d	Lower die's diameter, *mm*
d_p	Punch's diameter, *mm*
E	Young's modulus, *MPa*
f	Porosity or void volume fraction
f_0	Initial void volume fraction
f_c	Critical void volume fraction
f_F	Void volume fraction at failure
f_N	Void nucleation volume fraction
n	Hardening exponent of the material
q_1, q_2	Coefficients of the GTN damage model
r	Fillet radius of lower die, *mm*
S	Standard deviation of ε_n
t	Specimen's thickness, *mm*
v	Punch drop rate, *mm/min*
δ	Rate of coalescence
ε_n	Mean strain for nucleation
μ	Friction coefficient
v	Poisson's ratio
$\sigma_{0.2}$	Conventional yield stress, *MPa*

2. Material and Pre-cracked SPT specimens

The material used in this study was a precipitation hardened martensitic stainless steel, 15.5PH. The elastoplastic behavior of the material was determined using standard tensile tests, in accordance with ASTM E 8M [7]. Young's modulus E, conventional yield stress $\sigma_{0.2}$, and the Ramberg-Osgood hardening exponent n were determined from the experimental stress-strain curve. The obtained results are shown in Table 1. The steel exhibits an isotropic behavior, close to that of an elastic-perfectly plastic material.

Table 1. Elastoplastic parameters of 15.5 PH steel

E (*MPa*)	v	$\sigma_{0.2}$ (*MPa*)	n
200000	0.3	1100	38.8
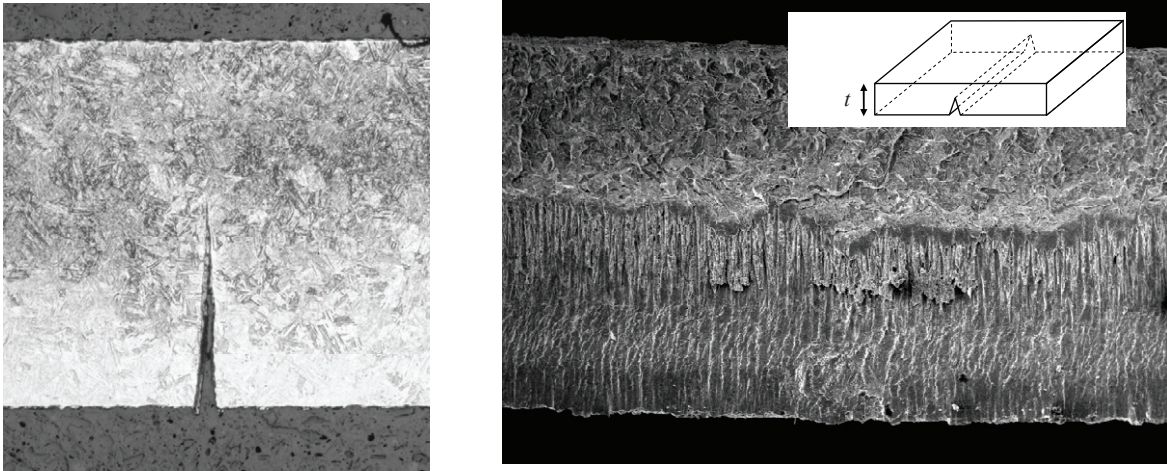
Fig. 1. Laser induced microcracking

The SPT specimens were obtained by slicing a part to produce 20x20x1mm square specimens. The laser-induced microcracks were obtained in 25 passes, using a $30 \mu m$ diameter Nd:YAG pulse beam ($50W$ and $1064nm$), working at a frequency of $7500Hz$ and a lineal displacement rate of $15mm/s$. A previous calibration is performed in order to adjust the power of the laser to achieve the desired crack depth on the specimen. The crack is made longitudinally from the center of one side of the specimen to the center to the opposite side . Figure 1 shows a cross section view of the initial crack obtained with this technique. Note that the crack obtained is a sharp crack, resembling a perfect crack without a rounded tip, but nevertheless the crack front is irregular, as it is shown in Figure 1, where the depth of the crack is seen to vary significantly along its length, leaving peaks and valleys as the laser advances. The variability of the crack front depth obtained using this technique was estimated to be around 10%.

A punch with semi-spherical head of diameter of $d_p = 5mm$ has been used to perform the test, while the hole in the lower die has a diameter of $D_d = 8mm$ and a fillet radius of $r = 1mm$. The test was performed at room temperature. The tests were displacement controlled with a punch drop rate of $v = 0.2mm/min$. Several specimens have been obtained with different a/t ratios from 0.2 to 0.5. The typical experimental curves (load vs. punch displacement) for the different tests are presented in Figure 2.
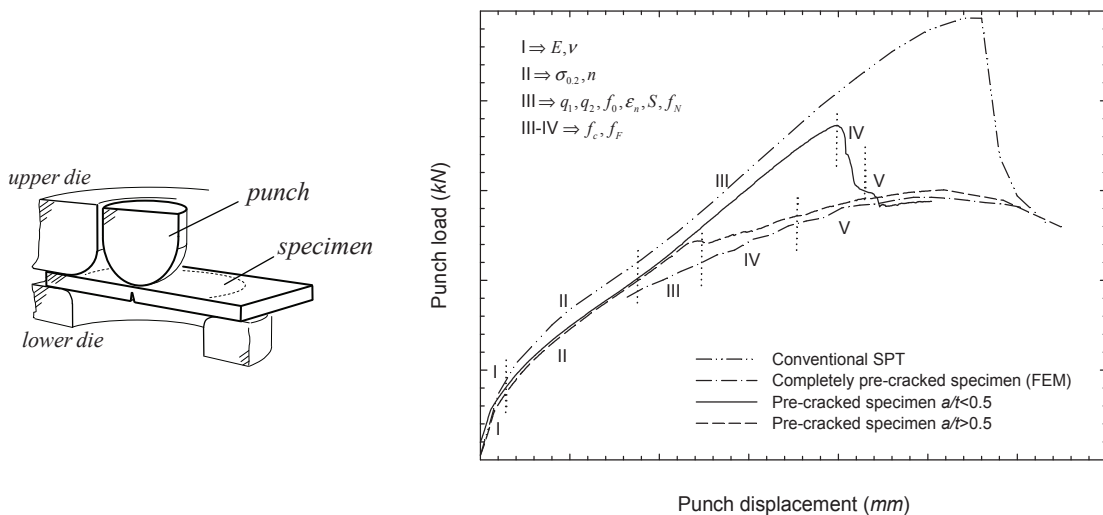
Fig. 2. Test apparatus and a typical P-SPT load displacement curves for different initial crack sizes

3. The GTN damage model

The micromechanical model, developed by Gurson-Tvergaard-Needleman (GTN) has been used, because it allows the different stages of ductile fracture, namely (nucleation, growth and coalescence of microvoids) to be recorded and distinguished by means of different damage constitutive parameters. The original Gurson model [8,9] considered a damaged material as a continuum medium with a different constitutive equation that includes a damage parameter called porosity f, which may vary from zero for undamaged material to one for completely damaged material.

The main drawback of this model is its inability to predict the final instability caused by the coalescence of microvoids in the final stage of ductile fracture. As a consequence, the original Gurson model was modified by Tvergaard and Needleman [10-12] and can be expressed as follows:

$$F = \left(\frac{\bar{\sigma}}{\sigma_y}\right)^2 + 2q_1 f^* \cosh\left(\frac{q_2 \sigma_{kk}}{2\sigma_y}\right) - \left[1 + \left(q_1 f^*\right)^2\right] = 0 \qquad (1)$$

Where σ_{kk} is the first invariant of stress state, $\bar{\sigma}$ is the Von Mises equivalent stress, and σ_* is the flow stress of the matrix. The model coefficients proposed by Tvergaard and Needleman to amplify the hydrostatic stress effect for all strain levels are q_1 and q_2, with a reasonable constant value for metals [13,14] of $q_1 = 1.5$ and $q_2 = 1.0$. Finally, f^* is the modified void volume fraction that takes into account the final decrease in load when void coalescence occurs,

$$
\begin{aligned}
f^* &= f &\quad \text{if } f \leq f_c \\
f^* &= f_c + \delta\left(f - f_c\right) &\quad \text{if } f > f_c
\end{aligned}
\qquad (2)
$$

Here, f is the volumetric fraction of voids or porosity, f_c is the critical porosity from which the interaction between voids and the coalescence process starts, and δ is the rate of coalescence of the microvoids. The rate of coalescence δ can be obtained from the void volume fraction when the material fails, f_F:

$$\delta = \frac{f_u^* - f_c}{f_F - f_c} \qquad (3)$$

The above equations establish the behaviour of a material when a specific porosity value is considered. However, as the material is subjected to progressively higher levels of strain, the porosity also increases. There are two phenomena which combine to produce the increase in porosity. On the one hand, the existing microvoids gradually grow, resulting in an increased volumetric fraction, and on the other, new microvoids are generated in the material as a result of the greater plastic strains. As a consequence, if considering a strain-controlled nucleation, the increase in porosity can be written as:

$$\dot{f} = \dot{f}_{growth} + \dot{f}_{nucl} = \left(1 - f\right)\dot{\varepsilon}_{kk}^p + \frac{f_N}{S\sqrt{2\pi}}\exp\left[-\frac{1}{2}\left(\frac{\varepsilon_m^p - \varepsilon_n}{S}\right)^2\right]\dot{\varepsilon}_m^p \qquad (4)$$

Here the growth of the existing voids is controlled by the trace of plastic strain increment tensor $\dot{\varepsilon}_{kk}^p$, and the nucleation of new voids depends on (a) ε_n, the mean strain for nucleation, (b) f_N, the void nucleation volume fraction that controls the void volume fraction when the nucleation begins, (c) S the standard deviation of ε_n and (d) f_0, the initial void volume fraction. In this work a typical value of $S = 0.01$ has been assumed, and not initial damage has been considered, so $f_0 = 0$, but it is generated along the specimen deformation process.

4. Numerical procedure

In the P-SPT load-displacement curve up to five zones can be distinguished (Figure 2). Each of the necessary material parameters $(E, v, \sigma_{0.2}, n)$ and damage parameters $(q_1, q_2, f_0, \varepsilon_n, S, f_N, f_c, f_F)$ starts its influence in the test at different stages:

- Region I. This zone is mainly controlled by the elastic material properties. Parameters of influence are E and v. The curve almost becomes a straight line.
- Region II. This zone reflects the transition between the elastic and the plastic behaviour. Parameters of influence here are $\sigma_{0.2}$ and n.
- Region III. Here the whole specimen has a pure plastic behaviour in the fracture process zone. The void nucleation begins where bigger plastic strain occurs. Parameters of influence are $q_1, q_2, f_0, \varepsilon_n, S$ and f_N. The volume void fraction grows as the punch displacement does. The crack initiation takes place along this stage when the void volume fraction takes the value f_c in the centre of the specimen. Crack develops through the thickness.
- Region IV. The crack develops until the complete thickness is broken under the punch, and then the maximum load is reached. The parameter δ has influence in this stage as the crack growth takes place.
- Region V. This is the final failure zone. The crack grows from the centre to the borders of the specimen. The parameter δ is related to the decreasing speed of the curve.

In a previous work, interrupted tests (Figure 3) at different load levels have been performed in order to obtain the value for crack initiation in the region III [15]. A value of the 85% of the maximum load can be considered as a representative value for material.

In this work, for the numerical simulations the FE code ABAQUS Explicit was used. As a consequence of the symmetrical geometry, with respect of the YZ and ZX planes, only a quarter of the specimen needs to be modelled. The punch and the fillet radius of the lower die were considered as rigid parts for the simulation. The specimen has been modelled with 8-node brick type elements. A mesh size of $0.05\,mm$ has been used in the process zone, where the crack initiation occurs. Figure 4 show the typical mesh used for a damage analysis.

The friction coefficient (μ) between the different parts was also be taken into account in the simulation [16]. A typical value for steel-steel contact of $\mu = 0.18$ was used.

The experimental data from the true stress-strain curve were used to obtain the elastic and plastic behaviour of the undamaged material (Table 1). The uniaxial plastic behaviour of the material for large strains is considered as an extrapolation of their behaviour prior to necking, using a Ramberg-Osgood adjustment.
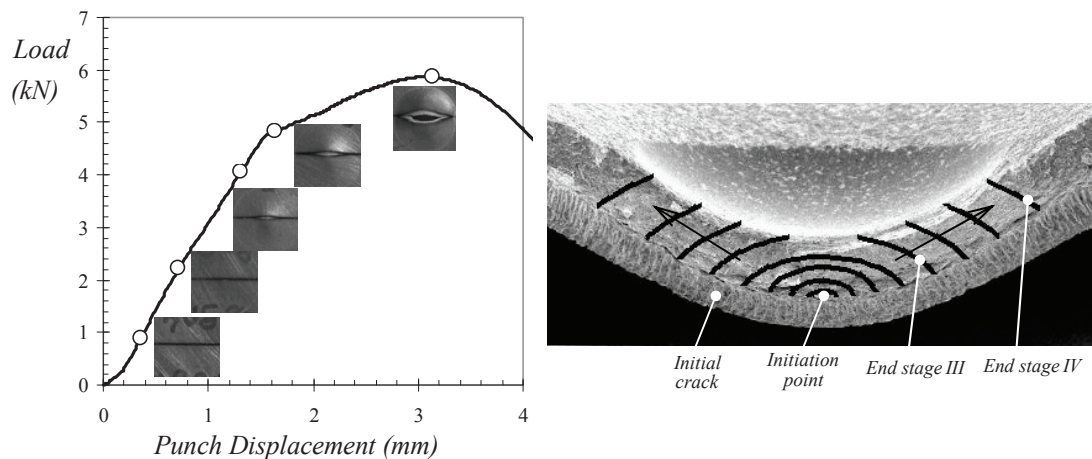
Fig. 3. Interrupted tests, showing the initiation area, and the different stages of the cracking process.
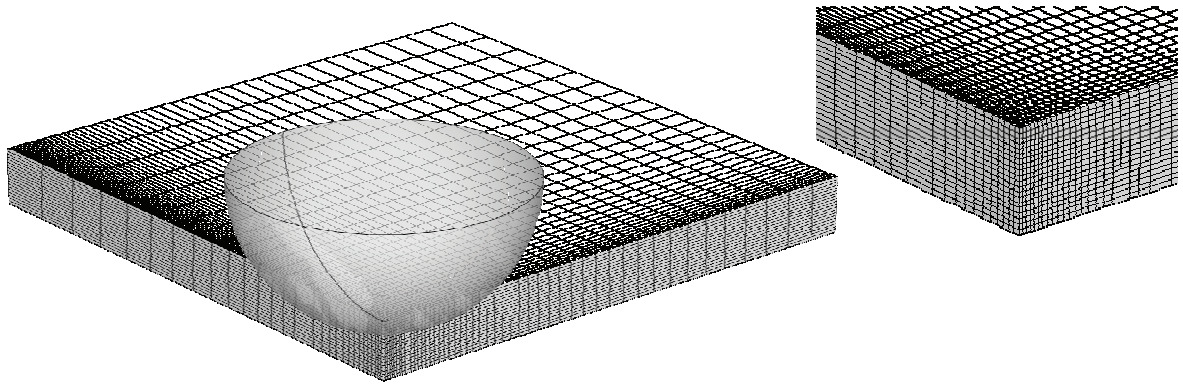
Fig. 4. Typical mesh of the P-SPT specimen for the numerical simulations of the damage evolution

Keeping in mind the above considerations, the material's damage parameters can be determined by adjusting the different regions on the load-displacement curve of the P-SPT tests. The recommendations in Tvergaard [10-12] were followed when setting the values of the constituent parameters $q_1 = 1.5$ and $q_2 = 1$. The initial porosity parameter can be considered negligible in this material, $f_0 = 0$, and the initial porosity deformation was established based on the instability value of the stress test, $\varepsilon_n = 0.1$, with a normal distribution $S = 0.01$. Consequently, the only values left to determine are those of f_N, f_c and f_F.

4.1. Variation in f_N

The parameter f_N dictates the shape of the curve in the first part of region III (segment between the end of region II and the instant at which propagation starts, at around 85% of maximum load) [17], since the remaining parameters on which this segment depends remain constant. The variation in the value of f_N was studied in the range [0.001, 0.015], which is typical for most steels [13,14]. Figure 5 shows the variation in region III for the range defined for f_N in the numerical simulations, and reveals that said variation is not significant and is very similar to the experimental scatter in region III, which is around 2%. This fact indicates that a one order of magnitude variation in f_N does not translate into a similar variation in the shape of the curve in region III, thus making a direct determination of f_N impossible.
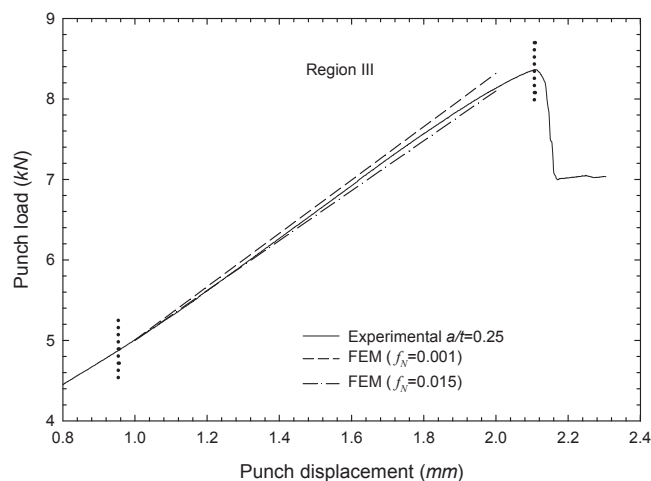
Fig. 5. Variation in region III for the range defined for f_N in the numerical simulations

4.2. Variation in f_F

The start of crack propagation in the specimen during the test is related to the coalescence of microvoids, that is, to when the volumetric fraction of microvoids reaches the value of f_F. In this experimental test, the instant of crack propagation was able to be determined using various techniques [16]. As already noted, its value is around 85% of the maximum load. For the sample shown in this analysis, this initiation value corresponds to a punch displacement of $1.75\,mm$. As a consequence, the evolution of the volumetric fraction of microvoids in the central region of the specimen (Figure 6) can be graphed versus punch displacement for each of the f_N values analyzed.

The value of f_F associated with each value of f_N can be determined using Figure 6. Finding the value for the punch displacement at the start of crack propagation ($1.75\,mm$) on the x-axis yields the volumetric fraction of microvoids at that instant. It can be observed that each f_N is associated with a different value of f_F. Table 2 lists these value pairs, referenced using the letters A to E.
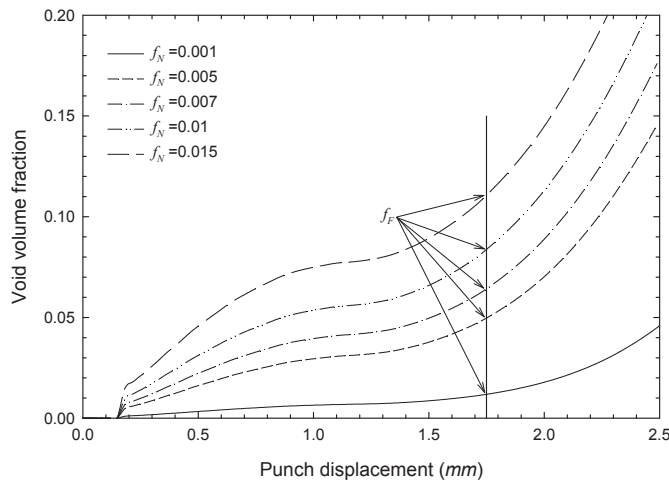
Fig. 6. Accumulated porosity in the central area for different values of f_N

Table 2. Values of f_N, f_F and f_c analyzed

f_N	f_F	Ref.	δ=7.5	δ=10	δ=12.5	δ=15	δ=17.5	δ=20	δ=22.5	δ=25	δ=30	δ=75	δ=100
								f_c					
0.001	0.012	A	-	-	-	-	-	-	-	-	-	**0.003**	0.005
0.005	0.05	B	-	-	-	0.006	0.013	**0.018**	0.021	0.024	0.037	0.042	0.044
0.007	0.065	C	-	-	0.013	**0.022**	0.029	0.033	0.037	0.040	0.053	0.057	0.059
0.01	0.083	D	-	0.018	**0.032**	0.041	0.048	0.052	0.056	0.059	0.071	0.075	0.077
0.015	0.111	E	0.026	**0.049**	0.063	0.071	0.077	0.082	0.085	0.088	0.100	0.103	0.105

4.3. Variation in f_c

Once the value pairs for f_N and f_F are determined, the value of f_c is given by expression (3) as a function of the microvoid coalescence speed δ, which was varied within the range [7.5,100]. Table 2 lists the different combinations for the parameters f_N, f_F and f_c, which were numerically analyzed and simulated. For each f_N - f_F pair, the optimum value of f_c was identified that best reproduced the experimental results of the P-SPT specimen with the ratio $a/t = 0.25$. These values are in bold type in Table 2. The resulting good fit can be seen in Figure 7 (set of values for reference C). These parameter sets were also verified to yield accurate representations of the behavior exhibited by other P-SPT specimens with different a/t ratios, since the triaxiality is very similar in all of them.
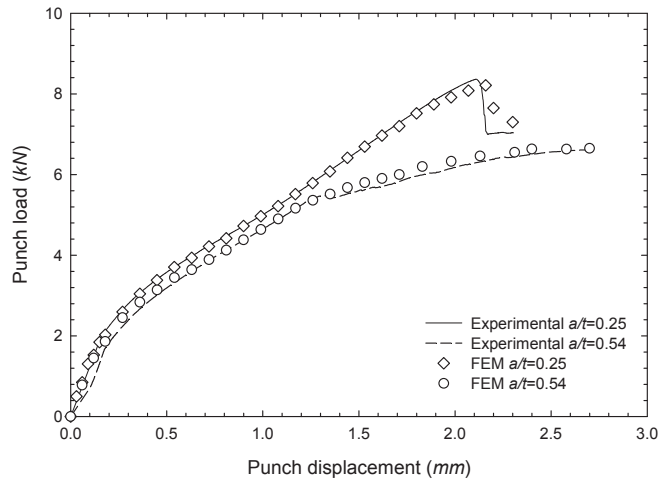
Fig. 7. Comparison of experimental-simulation results (set of values for reference C)
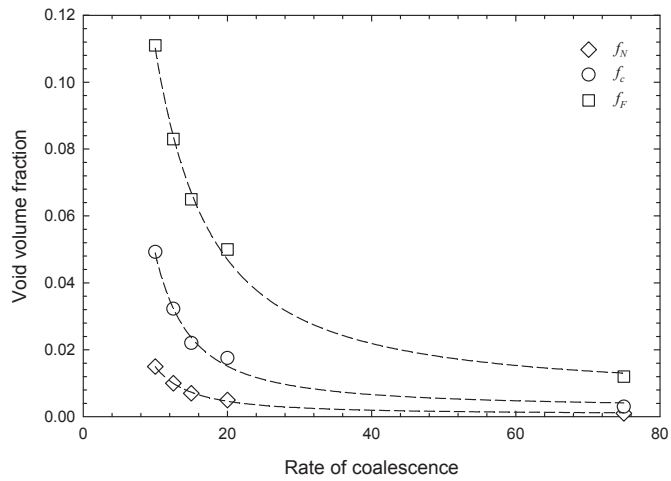
Fig. 8. Porosity curves as a function of coalescence speed
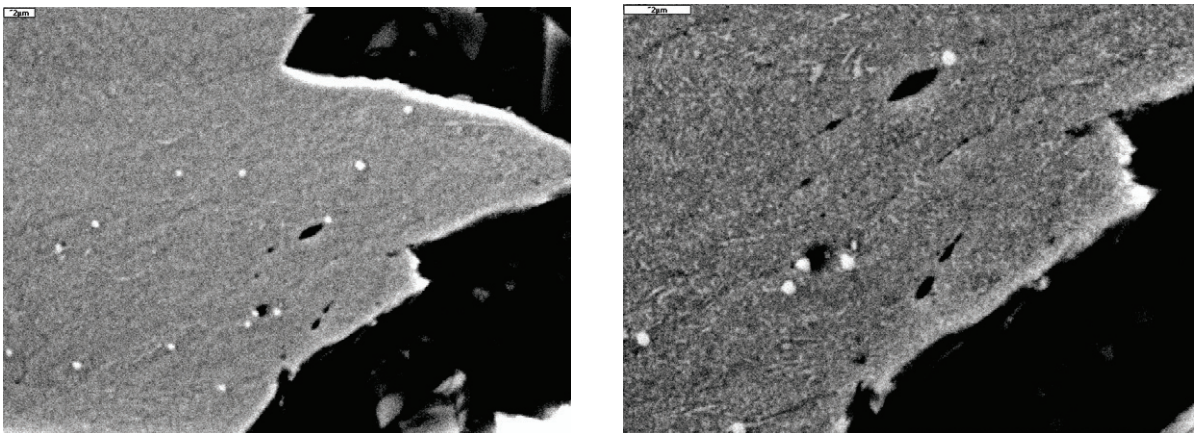
Fig. 9. Aspect of microvoids at the crack initiation zone.

Using the above results, a number of curves can be represented (Figure 8) that provide the values of the damage parameters (f_N, f_c and f_F) suitable for simulating the macroscopic behaviour of the P-SPT specimens. It can be observed as more than one set of values is able to simulate numerically the experimental load-displacement curves of the specimens P-SPT.

However, only one of the solutions presented in Figure 8 will be the characteristic one of the material. According to this, a suitable method for the identification of the real parameters of the material must be established. This unique solution will have a physical meaning, directly related to the microstructure and damage evolution of the material. A first attempt could be to obtain some of the damage parameters (f_N, f_c and f_F) using an experimental technique, so the rest is already determined from the relationships established in Figure 8.

In this sense, a fractographic analysis has been carried out with the aim of determining the critical porosity when fracture occurs. The results show the great difficulty of extracting a damage parameter (eg. critical porosity), with a certain level of reliability, from this fractographic analysis (Figure 9). Damage at the crack tip is very located, and the crack advances throughout the area when voids are generated. In addition, voids appear crushed due to the high pressure exerted by the punch.

5. Conclusions

In this paper, a methodology to obtain the damage parameters of the P-SPT specimens has been established. It was observed that there is a set of different solutions suitable for simulating the macroscopic behavior of the specimens, when using the GTN damage model. From a numerical point of view, any of them can be used but physically only one is correct. In this sense, a fractographic analysis has been effected in some P-SPT specimens after test.

The results show the difficulty to extract a damage parameter, with some level of reliability, based on a fractographic analysis of the process zone for these P-SPT specimens. As a result, testing of P-SPT specimens, appear to be insufficient to determine a set of damage parameters associated with the microstructure of the material. In any case, the methodology presented allows the damage parameter sets, able to simulate the behaviour of these specimens, to be obtained.

Acknowledgements

References

[1] Mao X, Takahashi H. Development of a further-miniaturized specimen of 3 mm diameter for tem disk small punch tests. *J. Nucl. Mater.* 1987;**150**:42–52.

[2] Mao X, Takahashi H, Kodaira T. Supersmall punch test to estimate fracture toughness Jic and its application to radiation embrittlement of 2.25Cr-1Mo steel. *Mater. Sci. Eng.* 1992;**AI50**:231–6.

[3] Baik J-M, Kameda J, Back O. Small Punch Test evaluation of intergranular embrittlement of an alloy steel. *Scr. Metallurgica et Materialia* 1983;**17**:1443–7.

[4] Ju J-B, Jang J, Kwon D. Evaluation of fracture toughness by small-punch testing techniques using sharp notched specimens. *Int. J. of Press. Vessels Pip.* 2003;**80**:221–8.

[5] Cuesta II, Alegre JM, Lacalle R, Álvarez JA, Gutiérrez-Solana F. Cálculo de la integral J en probetas SPT para la estimación de la tenacidad a fractura. *Anales de Mecánica de la Fractura* 2008;**25**:486–91.

[6] Cuesta II, Alegre JM, Bravo PM. Evaluación de la tenacidad a fractura mediante la combinación del diagrama FAD y de ensayos SPT sobre probetas fisuradas. *Anales de Mecánica de la Fractura* 2009;**26**:382–7.

[7] ASTM E 8M. Standard Test Methods of Tension Testing of Metallic Materials [Metric]. *Annual Book, American Society for Testing and Materials* 2003;Vol. 3.01.

[8] Gurson AL. Continuum theory of ductile rupture by void nucleation and growth: Part I – Yield criteria and flow rules for porous ductile materials. *J. Eng. Mater. Technol.* 1977;**99**:2–15.

[9] Gurson AL. Proc. Int Conf. Fracture. Pergamon Press. Oxford 1977;**2**:357–64.

[10] Tvergaard V. Material Failure by Void Growth to Coalescence. In: Advances in Applied Mechanics. Academic Press Inc; 1990;**27**:83–151.

[11] Tvergaard V, Needleman A. An Analysis of Ductile Rupture in Notched Bars. *Acta Metall.* 1985;**32**:157–69.

[12] Needleman A, Tvergaard V. An analysis of dynamic, ductile crack growth in a double edge cracked specimen. *Int. J. Fract.* 1991;**49**:41–67.

[13] Abendroth M, Kuna M. Determination of deformation and failure properties of ductile materials by means of the Small Punch test and neural networks. *Computational Mater. Sci.* 2003;**28**:633–44.

[14] Benseddiq N, Imad A. A ductile fracture analysis using a local damage model. *Int. J. of Press. Vessels Pip.* 2008;**85**:219–27.

[15] Cuesta II. Evaluación de la tenacidad a fractura en aceros mediante el uso de probetas miniatura prefisuradas. *Tesis Doctoral.* Universidad de Burgos; 2010.

[16] Autillo J, Contreras MA, Betegón C, Rodríguez C, Belzunce FJ. Utilización del ensayo miniatura de punzonamiento (Small Punch Test) en la caracterización mecánica de aceros. *Anales de Mecánica de Fractura* 2006;**23**:77–83.

[17] Cuesta II, Alegre JM, Barbáchano H. Utilización del modelo de daño de Gurson-Tvergaard para la simulación del ensayo small punch sobre probetas prefisuradas. *XII Congreso Nacional de Propiedades Mecánicas de Sólidos* 2010; p. 146–155.